Article:

ORIGINAL PAPER

Detection of acetone vapours using solution-processed tin oxide thin-film transistors

Lauren R. Miller[1] · Robert J. Borthwick[1] · Paloma L. dos Santos[1] · Mujeeb U. Chaudhry[1]

© The Author(s) 2023

Abstract
Abnormal concentrations of volatile organic compounds (VOCs) in human breathe can be used as disease-specific biomarkers for the non-invasive diagnosis of medical conditions, such as acetone for diabetes. Solution-processed bottom gate top contact metal oxide thin-film transistors (TFTs) are used to detect acetone vapours, as part of a proof-of-concept study. The effect of increasing annealing temperature (T) and channel length (L) on electrical and sensing performance are explored. Drain current (I_{ds}) increases following exposure as acetone undergoes a redox reaction with the adsorbed oxygen species on the semiconductor surface, which results in free electrons being released back into the conduction band. Responsivity (R) is maximized at negative bias ($V_{gs} < 0$). For $L = 50$ μm, the peak R of the TFT annealed at 450 °C is three times greater than that of the TFT annealed at 350 °C, with $V_{gs} = -37.5$ V and -33 V, respectively.

Introduction

The remote detection of chemical vapours, specifically volatile organic compounds (VOCs), is paramount to public health and environmental monitoring. The detection of acetone in human breathe is useful for the non-invasive and real-time diagnosis of diabetes. The concentration of acetone from a healthy individual varies from 0.3 to 0.9 ppm and exceeds 1.8 ppm for a diabetic patient [1, 2]. Common sensing technologies such as gas chromatography, mass spectrometry and optical spectroscopy are costly, bulky and require a skilled technician [3, 4]. Therefore, investigating new devices that are compact, simple to operate, and can detect sub-ppm traces of VOCs with high selectivity and specificity, under a highly humid environment (relative humidity (RH) > 80% [5]), is critical. Chemiresistive gas sensors based on highly abundant metal oxides, such as SnO₂, are well publicised due to their miniaturized size, ease of fabrication and long-term stability [6, 7]. The sensing mechanism is reversible and involves monitoring changes in surface resistance following exposure to analytes of interest [8]. Several groups have developed highly sensitive exhaled breath sensors that incorporate 1D nanostructures, owing

to their high surface-to-volume ratio and open porosity. For example, Shin et al., obtained short response (< 11 s) and recovery times (< 6 s) upon exposure to acetone and humid air by combining Pt catalytic nanoparticles with SnO₂ fibres [5]. However, accurate cross-sensitivity toward exhaled breath containing multiple gases such as acetone, toluene and H₂S remains a major challenge.

Metal oxide semiconductor field effect transistors (MOSFETs) have been widely reported to detect acetone vapours and other harmful gases (e.g., NO₂) via two distinct sensing mechanisms [9, 10]. In contrast with chemiresistive gas sensors, current modulation by the gate electrode yields an amplified response and cross-sensitivity can be improved by operating the MOSFET in depletion or enhancement modes. Changes in other electrical parameters such charge carrier mobility (μ) and threshold voltage (V_{th}) can also be exploited. For example, Andringa et al., deposited ZnO thin films by spray pyrolysis and source-drain electrodes were patterned using photolithography, resulting in finger transistors. I_{ds} decreased upon exposure to NO₂ and an applied positive bias ($V_{gs} > 0$), which caused a shift in V_{th} for concentrations as low as 10 ppb [9].

Considering the aforementioned points, solution-processed bottom gate top contact (BGTC) single layer SnO₂ TFTs were used to detect acetone vapours under ambient conditions. Source-drain electrodes were deposited via thermal evaporation, which is simple, ideal for large batch processing and can achieve high deposition rates. The effect of

✉ Lauren R. Miller
  lauren.r.miller@durham.ac.uk

1   Department of Engineering, Durham University, Lower Mountjoy, South Rd, Durham DH1 3LE, UK

increasing T and L on electrical and sensing performance were explored. I_{ds} increased following exposure as acetone underwent a redox reaction with the adsorbed oxygen species on the semiconductor surface, which resulted in free electrons being released back into the conduction band.

To the best of our knowledge, this is the first study examining the use of SnO$_2$ TFTs to detect acetone vapours and will be pivotal in developing novel exhaled breath sensors.

Materials and methods

Experimental and characterisation techniques were conducted under ambient conditions, unless otherwise stated. The thermal behaviour of the sol–gels was examined using thermal gravimetric analysis (TGA) (Perkin Elmer Pyris 1 TGA) at a ramp rate of 10 °C min^{-1} from 30 to 500 °C. The crystalline properties of the films were determined using X-ray diffraction (XRD) (Bruker AXS D8 Advance GX003410) and surface morphology examined by atomic force microscopy (AFM) (Asylum Research MFP-3D Infinity). AFM analysis was performed by open-source software, Gwyddion. The electrical performance of the TFTs was characterised using Agilent B2912A source measurement units (SMUs) and probe station. A bespoke chamber (Fig. 3d) was manufactured to record changes in transfer characteristics upon exposure to analytes.

Calculation of saturation and effective mobility

Differences in I_{ds} following exposure to analytes are caused by effects on μ and V_{th}. Assuming that μ is independent of V_{gs} and neglecting short channel effects, I_{ds} in the saturation regime is given by Eq. (1) [11]:

$$I_{ds} = \frac{WC_i}{2L}\mu\left(V_{gs} - V_{th}\right)^2, \tag{1}$$

where I_{ds} is the drain current, $\frac{W}{L}$ is the channel width-to-length ratio, C_i is the capacitance per unit area of the dielectric layer, μ is the charge carrier mobility, V_{gs} is the gate voltage and V_{th} is the threshold voltage. μ is obtained by taking the partial derivative with respect to V_{gs}. Rearranging the resulting equation yields Eq. (2):

$$\mu = \frac{2L}{WC_i}\left(\frac{\partial\sqrt{I_{ds}}}{\partial V_{gs}}\right)^2. \tag{2}$$

$\frac{\partial\sqrt{I_{ds}}}{\partial V_{gs}}$ can be extracted by plotting $\sqrt{I_{ds}}$ against V_{gs} and finding the gradient. Ideal transfer characteristics are linear and hence $\frac{\partial\sqrt{I_{ds}}}{\partial V_{gs}}$ is constant. In practice, external factors such as contact resistance can produce curved plots, which has

resulted in a several erroneous reported mobilities. The reliability factor (r) given in Eq. (3) accounts for nonlinearities in transfer characteristics [11]. It is defined as the ratio (expressed in %) of the maximum channel conductivity experimentally achieved in a FET to that calculated in an equivalent ideal FET:

$$r = \frac{\left(\dfrac{\sqrt{|I_{ds}|^{max}} - \sqrt{|I_{ds}|^0}}{|V_{gs}|^{max}}\right)^2}{\left(\dfrac{WC_i}{2L}\mu\right)^2_{claimed}}, \tag{3}$$

where $\left(\frac{WC_i}{2L}\mu\right)^2_{claimed}$ accounts for the claimed device parameters and mobility in the saturation regime. $|I_{ds}|^{max}$ is the experimental maximum drain current reached at the maximum gate voltage, $|V_{gs}|^{max}$. $|I_{ds}|^0$ is the drain current at $V_{gs} = 0$. Effective mobility, μ_{eff}, is thus given by:

$$\mu_{eff} = \mu \times r. \tag{4}$$

The values quoted in this report are μ_{eff} and calculated using $C_i = 15$ nFcm^{-2} and $W = 1$ mm. $L = 50, 80, 100$ and 120 µm unless otherwise stated.

Transistor fabrication

The SnO$_2$ sol–gel was prepared from anhydrous SnCl$_2$ that was dissolved in 2-methoxyethanol (10 mL, 0.15 M). The solution was sonicated for 15 min, stirred for 24 h to promote hydrolysis and passed through a syringe fitted with a 22 µm filter prior to spin-coating. The SnO$_2$ sol–gel was spin-coated at 5000 RPM for 30 s onto pre-cleaned substrates consisting of a 400 nm SiN$_x$ dielectric on a highly doped Si wafer, which acted as the back gate. The samples were annealed at 350 °C or 450 °C for 1 h and finally, 50 nm thick Al source-drain electrodes were deposited via thermal evaporation using a shadow mask under high vacuum ($\approx 10^{-6}$ mbar) in a system integrated in a nitrogen glovebox. The mask comprised four transistors with variable channel lengths, $L = 50, 80, 100$ and 120 µm.

The phase transitions of a sol–gel during high temperature annealing can be observed by monitoring the weight change that occurs when a sample is heated at a constant rate. Initially, metal-hydroxide (M–OH) or metal–oxygen (M–O) bonds are created, which is referred to as a hydrolysis reaction. As temperature is increased, condensation and dehydroxylation remove the remaining impurities to generate metal-oxide-metal (M–O–M) bonds. The lattice becomes denser, which can lead to a phase transition from amorphous to polycrystalline by means of an exothermic reaction [12, 13]. A TGA curve from the SnO$_2$ sol–gel is shown in Fig. 1. The derivative of the curve is plotted to highlight the
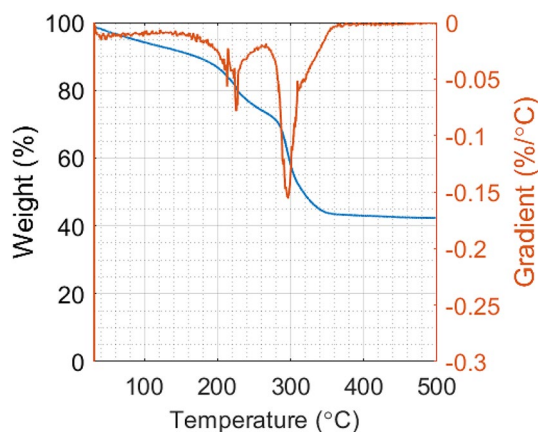
Fig. 1 TGA curve and derivative plot of SnO_2

temperature range at which each process occurs. The weight reduction prior to 200 °C was attributed to the evaporation of the organic solvent, 2-methoxyethanol, which has a boiling point of 124 °C. No further weight loss was recorded after 450 °C, which indicated that a dense M–O–M network had formed.

Acetone sensing in air

An open 3 mL vial was filled with acetone and placed in a sealed custom-built chamber (Fig. 3d), which was then allowed to form a saturated atmosphere overnight. When I_{ds} plateaued, the taps on the chamber were opened in a fume cupboard. The TFT was removed and heated at 100 °C for 1 h under ambient conditions to recover I_{ds}. R was calculated using Eq. (5) for each TFT:

$$R = \frac{\Delta I_{ds}}{I_{ds}[0]} = \frac{I_{ds}[\text{analyte}] - I_{ds}[0]}{I_{ds}[0]}, \tag{5}$$

where ΔI_{ds} represents the difference in I_{ds} before ($I_{ds}[0]$) and after ($I_{ds}[\text{analyte}]$) exposure to acetone vapours.

Results

Optimisation of TFT charge transport layer

Single layer SnO_2 TFTs were fabricated and characterised to investigate the effect of increasing T and L on electrical performance. The device structure and the corresponding transfer characteristics for the TFTs annealed 350 °C and 450 °C are shown in Fig. 2a and b, respectively.

XRD analysis of the film annealed at 450 °C showed peaks at $2\theta = 26.6°$ and 33.9° (Fig. 2c) consistent with the (110) and (101) crystal planes of SnO_2 [14]. The

corresponding AFM image (Fig. 2d) suggested that the film was polycrystalline, which would have allowed the M–O–M backbones in the metal oxide to serve as electron conductance pathways between atoms. The maximum grain size and root mean square (rms) roughness were calculated from the AFM image as 32.2 nm and 1.28 nm, respectively, which indicated a high-quality morphology.

Conversely, XRD and AFM analyses of the film annealed at 350 °C (Fig. S2) suggested that the film was amorphous, as the maximum grain size and rms roughness were calculated as 7.4 nm and 0.340 nm, respectively.

Maximum drain current ($I_{ds\ [max]}$) and μ_{eff} increased with T for all L (Table 1 ($L = 50$ μm) and S1 ($L = 50, 80, 100$ and 120 μm). The output characteristics (Fig. S1) show that high I_{gs} was present, as the curves shifted right with increasing V_{gs}.

Acetone sensing in air

Following exposure to acetone vapours, I_{ds} of the SnO_2 TFTs were examined in both depletion and enhancement modes. I_{ds} for both devices ($L = 50$ um) were monitored following overnight exposure, as shown in Fig. 3a and b. R was plotted against V_{gs} (Fig. 3c) for $L = 50, 80$ and 100 μm.

Discussion

The substantial improvement in μ_{eff} and $I_{ds\ [max]}$ with increasing T may have been owing to a greater proportion of M–O–M bonds, which are known to result in a highly ordered and dense lattice. It is likely that the TFT annealed at 350 °C would have contained a greater proportion of M–OH bonds due to incomplete dehydroxylation and condensation, which acted as traps and hence hindered electron transport [15].

Table S1 suggested that $I_{ds\ [max]}$ decreased with increasing L, as the resistance of the channel is inversely proportional to the width-to-length ratio. Therefore, I_{gs} was dominant at larger L and less charges were able to accumulate at the semiconductor-dielectric interface.

Chen et al., found that acetone acts as a reducing agent that transfers electrons to the SnO_2 (110) surface [15]. The sensing mechanism is shown in Eqs. (6)–(8). Due to the large electronegativity of oxygen atoms, adsorbed oxygen depletes electrons from the SnO_2 film, which increases its resistance and forms reduced oxygen species (O^{2-}, O_2^- or O^-, depending on temperature). The film resistance in air is therefore larger than in vacuum. Acetone undergoes a redox reaction with the reduced oxygen species, which results in free electrons being released back into the conduction band of SnO_2 [16].

Fig. 2 a Single layer SnO$_2$ TFT; **b** Transfer characteristics in the saturation regime at $V_{ds} = 40$ V, $V_{gs} = -40$ to 40 V and $L = 50$ μm for TFTs annealed at 350 °C and 450 °C. Leakage current (I_{gs}) is shown as dashed lines. **c** XRD analysis of TFT annealed at 450 °C for $2\theta = 5°$ to 60°. **d** AFM image of TFT annealed at 450 °C with 2 μm scan area
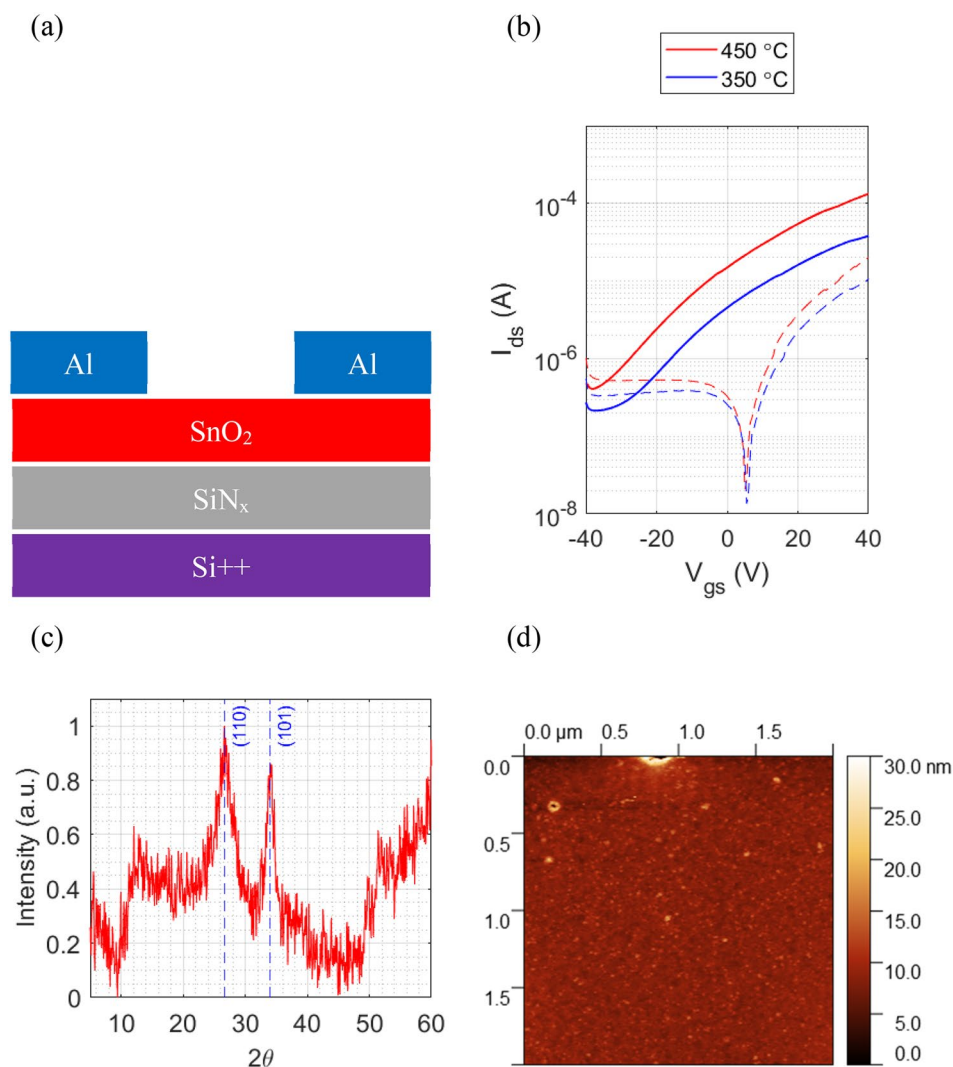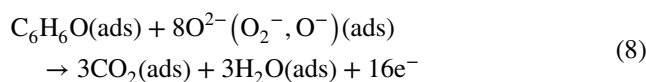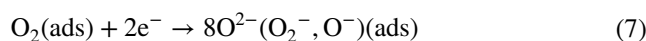

Table 1 Current on/off ratio ($I_{on/off}$), μ_{eff}, $I_{ds\,[max]}$ and V_{th} of SnO$_2$ TFTs annealed at 350 °C and 450 °C ($L = 50$ μm) before exposure, after exposure, and recovery

T (°C)	μ_{eff} (cm^{2}V^{-1} s^{-1})	$I_{on/off}$	$I_{ds\,[max]}$ (A)	V_{th} (V)
450				
Before exposure	0.246	3.26×10^2	1.33×10^{-4}	− 18.6
Acetone	0.329	3.75×10^0	1.62×10^{-3}	− 142
Recovery	0.140	3.12×10^2	4.86×10^{-5}	− 5.79
350				
Before exposure	0.0685	1.80×10^2	3.83×10^{-5}	− 19.0
Acetone	0.153	6.00×10^0	4.15×10^{-4}	− 94.6
Recovery	0.0677	8.48×10^2	3.12×10^{-5}	− 12.8

$$O_2(g) \rightarrow O_2(ads) \tag{6}$$

$$O_2(ads) + 2e^- \rightarrow 8O^{2-}(O_2^-, O^-)(ads) \tag{7}$$

$$C_6H_6O(ads) + 8O^{2-}\left(O_2^-, O^-\right)(ads)$$
$$\rightarrow 3CO_2(ads) + 3H_2O(ads) + 16e^- \tag{8}$$

I_{ds} increased following exposure to acetone vapours, as depicted in Fig. 3a and b. This was consistent with the conductivity of the film increasing due to surplus electrons donated by acetone. The increase in V_{th} (Table 1) suggested that excess electrons prevented normally off operation as the film was too conductive. R was maximized at negative bias ($V_{gs} < 0$) (Fig. 3c). For $L = 50$ μm, the peak R of the TFT annealed at 450 °C was three times greater than that of the TFT annealed at 350 °C, with $V_{gs} = -37.5$ V and − 33 V, respectively. The shape of the peak broadened with increasing L irrespective of T, which suggested that a high R can be achieved at the V_{gs} required for a battery-driven handheld sensor.

Fig. 3 **a** Transfer characteristics in the saturation regime at $V_{ds} = 40$ V, $V_{gs} = -40$ to 40 V and $L = 50$ μm, obtained before and after the TFTs annealed at 350 °C and. **b** 450 °C were exposed to acetone overnight. I_{gs} is shown as dashed lines. **c** R versus V_{gs} of the TFTs annealed at 350 °C and 450 °C for $L = 50$, 80, and 100 μm. 450–50 corresponds to $T = 450$ °C and $L = 50$ μm. **d** Testing chamber
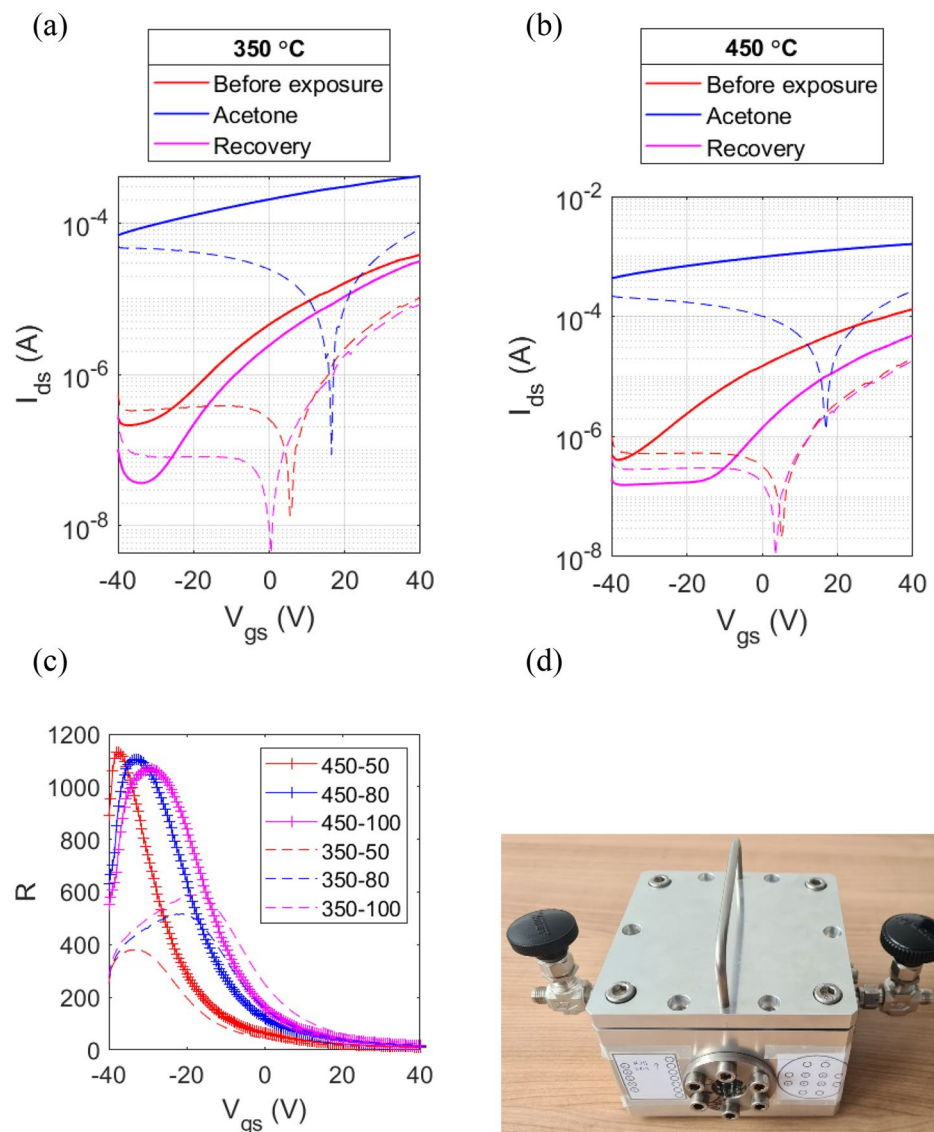
Oxygen species readsorbed to the SnO_2 surface during heating under ambient conditions. I_{ds} was recovered as the $I_{on/off}$ was comparable to that measured before exposure. V_{th} was also noticeably lower, which could be owing to the detrapping of electrons and increased density of conducting states.

To conclude, the TFT annealed at 450 °C ($L = 50$ μm) was more responsive to the presence of acetone vapours across the whole bias range than the TFT annealed at 350 °C, due to increased electron transport facilitated by a denser M–O–M network. AFM and XRD analyses indicated clear evidence of higher crystallinity with T. At smaller L, a greater density of charges were able to accumulate at the semiconductor-dielectric interface and promoted electron transfer between acetone and SnO_2. A new, improved vapour testing chamber is currently being designed, which will allow vapour concentration to be accurately determined. Testing and recovery under nitrogen will also be possible. This study could further benefit from Fourier transform infrared spectrometry (FT-IR) and X-ray photoelectron spectroscopy (XPS), which may confirm that the film annealed at 450 °C contained a greater fraction of M–O–M bonds. Differential scanning calorimetry (DSC) could also be performed to help identify the temperature range at which crystallization occurred. However, we believe that the results presented here are sufficient for this paper.

Going forward, SnO_2 TFTs annealed at T > 450 °C will be fabricated and characterised to investigate whether electrical and sensing performance can be further enhanced. These devices will be exposed to VOCs for the diagnosis of other conditions, such as toluene for lung cancer [17].

Data availability The datasets presented during this study are available from the authors on reasonable request.

Declarations

Conflict of interest There is no conflict of interest to declare.

References

1. S.-J. Choi et al., Selective diagnosis of diabetes using Pt-functionalized WO3 hemitube networks as a sensing layer of acetone in exhaled breath. Anal. Chem. **85**(3), 1792–1796 (2013). https://doi.org/10.1021/ac303148a

2. M. Righettoni, A. Tricoli, S.E. Pratsinis, Si:WO3 sensors for highly selective detection of acetone for easy diagnosis of diabetes by breath analysis. Anal. Chem. **82**(9), 3581–3587 (2010). https://doi.org/10.1021/ac902695n

3. M. Phillips et al., Volatile organic compounds in breath as markers of lung cancer: a cross-sectional study. Lancet **353**(9168), 1930–1933 (1999). https://doi.org/10.1016/S0140-6736(98)07552-7

4. G. Peng et al., Diagnosing lung cancer in exhaled breath using gold nanoparticles. Nat. Nanotechnol. (2009). https://doi.org/10.1038/nnano.2009.235

5. J. Shin et al., Thin-wall assembled SnO2 fibers functionalized by catalytic Pt nanoparticles and their superior exhaled-breath-sensing properties for the diagnosis of diabetes. Adv. Funct. Mater. **23**(19), 2357–2367 (2013). https://doi.org/10.1002/adfm.201202729

6. A. Vomiero, S. Bianchi, E. Comini, G. Faglia, M. Ferroni, G. Sberveglieri, Controlled growth and sensing properties of In2O3 nanowires. Cryst. Growth Des. **7**(12), 2500–2504 (2007). https://doi.org/10.1021/cg070209p

7. L. Wang, A. Teleki, S.E. Pratsinis, P.I. Gouma, Ferroelectric WO3 nanoparticles for acetone selective detection. Chem. Mater. **20**(15), 4794–4796 (2008). https://doi.org/10.1021/cm800761e

8. P.G. Harrison, M.J. Willett, The mechanism of operation of tin(iv) oxide carbon monoxide sensors. Nature (1988). https://doi.org/10.1038/332337a0

9. A.-M. Andringa, J.R. Meijboom, E.C.P. Smits, S.G.J. Mathijssen, P.W.M. Blom, D.M. de Leeuw, Gate-bias controlled charge trapping as a mechanism for NO2 detection with field-effect transistors. Adv. Funct. Mater. **21**(1), 100–107 (2011). https://doi.org/10.1002/adfm.201001560

10. K.-W. Kao, M.-C. Hsu, Y.-H. Chang, S. Gwo, J.A. Yeh, A sub-ppm acetone gas sensor for diabetes detection using 10 nm thick ultrathin InN FETs. Sensors **12**(6), 7157–7168 (2012). https://doi.org/10.3390/s120607157

11. H.H. Choi, K. Cho, C.D. Frisbie, H. Sirringhaus, V. Podzorov, Critical assessment of charge mobility extraction in FETs. Nat. Mater. **17**(1), 2–7 (2018). https://doi.org/10.1038/nmat5035

12. J.W. Park, B.H. Kang, H.J. Kim, A review of low-temperature solution-processed metal oxide thin-film transistors for flexible electronics. Adv. Funct. Mater. **30**(20), 1904632 (2020). https://doi.org/10.1002/adfm.201904632

13. G.H. Kim, H.S. Shin, B.D. Ahn, K.H. Kim, W.J. Park, H.J. Kim, Formation mechanism of solution-processed nanocrystalline InGaZnO thin film as active channel layer in thin-film transistor. J. Electrochem. Soc. **156**(1), H7 (2009). https://doi.org/10.1149/1.2976027

14. G. Huang, L. Duan, G. Dong, D. Zhang, Y. Qiu, High-mobility solution-processed tin oxide thin-film transistors with high-κ alumina dielectric working in enhancement mode. ACS Appl. Mater. Interfaces **6**(23), 20786–20794 (2014). https://doi.org/10.1021/am5050295

15. Y. Chen, H. Qin, Y. Cao, H. Zhang, J. Hu, Acetone sensing properties and mechanism of SnO2 thick-films. Sensors (2018). https://doi.org/10.3390/s18103425

16. H. Windischmann, P. Mark, A model for the operation of a thin-film SnO x conductance-modulation carbon monoxide sensor. J. Electrochem. Soc. **126**(4), 627–633 (1979). https://doi.org/10.1149/1.2129098

17. N.-H. Kim, S.-J. Choi, D.-J. Yang, J. Bae, J. Park, I.-D. Kim, Highly sensitive and selective hydrogen sulfide and toluene sensors using Pd functionalized WO3 nanofibers for potential diagnosis of halitosis and lung cancer. Sens. Actuators B **193**, 574–581 (2014). https://doi.org/10.1016/j.snb.2013.12.011